Available online at www.sciencedirect.com
ScienceDirect
Biosensors and Bioelectronics 23 (2008) 1298–1302
BIOSENSORS & BIOELECTRONICS
www.elsevier.com/locate/bios

Short communication

Label-free antibody–antigen binding detection by optical sensor array based on surface-synthesized gold nanoparticles

Rouslan V. Olkhov, Andrew M. Shaw *

School of Biosciences, University of Exeter, Stocker Road, Exeter EX4 4QD, UK

Received 23 August 2007; received in revised form 22 November 2007; accepted 23 November 2007
Available online 15 December 2007

Abstract

Gold nanoparticles grown *in situ* from printed seed particles on a glass substrate have been fabricated into a biosensor array. The light-scattering properties of the resulting surfaces show sensitivity to changes in the local refractive index. Each array spot is functionalized with fibrinogen or bovine serum albumin and scattered radiation is used to monitor the refractive index change on label-free binding of the antibodies to their antigens from whole blood antiserum. Data were collected real-time and the association rate constants for the specific antibody–antigen binding were derived from a kinetic analysis. The minimum antibody concentration detection sensitivity is of 100 nM.

Keywords: Nanoparticle; Array; Biosensor; Label-free detection; Light scattering; Antibody–antigen binding

1. Introduction

Nanoparticle-based biosensors have been suggested as a possible alternative to continuous-gold surface plasmon resonance sensors (McFarland and Duyne, 2003; Stuart et al., 2004). The strong optical extinction in the visible region of the electromagnetic spectrum exhibited by noble metal nanoparticles arises when the incident photon frequency is in resonance with a localised surface plasmon mode in the conduction band of the nanoparticles. The optical extinction has a contribution from both scatter and absorption with scattering dominating when spherical particles have a diameter greater than approximately 25 nm. The optical properties of the nanoparticles depend on their composition, shape, and size (Noguez, 2007) and therefore they may be tuned and optimised for a given application by nanoparticle-fabrication methods. Biosensor platforms based on the optical properties of nanoparticle arrays and even single particles have been used to monitor biological binding events without the need for a fluorescent marker (Haes et al., 2004; Heaton et al., 2001).

One evolving application of nanoparticle arrays and in particular label-free binding studies is in the field of high-throughput screening. The conventional instrumentation for high-throughput screening relies on fluorescently labelled markers and is capable of screening perhaps 10^4 compounds per day. However, although the fluorescent assay intensity information can be quantitatively correlated to concentrations, which is routinely realised in single-target techniques such as ELISA assays, the high-throughput screening is often limited only to "yes-no"—presence or absence of the biological molecule species, typically a protein or a gene. There is a large overhead in preparing the 10^4 different molecules for screening simply from the logistics of preparation of the plates and printing out the molecules and a more information-rich array screening technology is required.

Label-free surface plasmon detection techniques open a number of exciting possibilities for monitoring not just the presence or absence of a particular biomolecule but also to determine its absolute concentration. Further, an array allows the absolute concentrations of a number of molecules to be detected simultaneously to produce a pattern of molecular expression such as disease biomarkers, pointing towards a patient-specific treatment regimen. In contrast to the large body of work on nanoparticle-based platforms for single-target molecule analysis (Haes and Duyne, 2004), the techniques for simultaneous

* Corresponding author. Tel.: +44 1392 263495; fax: +44 1392 263434.
E-mail address: Andrew.M.Shaw@exeter.ac.uk (A.M. Shaw).
URL: http://www.ex.ac.uk/~amshaw0 (A.M. Shaw).

0956-5663/$ – see front matter © 2007 Elsevier B.V. All rights reserved.
doi:10.1016/j.bios.2007.11.023

monitoring multiple targets are less well developed. Most of the progress is achieved in surface plasmon resonance imaging, where protein concentration detection limit of ca. 1 nM was reported (Lee et al., 2006; Phillips et al., 2006) To our knowledge pure light-scattering techniques were not used in microarray imaging applications.

This work presents the fabrication of multiple-target sensor arrays based on gold nanoparticles and demonstrates its application in detecting two antibodies in whole antisera by using a light-scattering sensor array reader.

2. Experimental

Arrays of gold nanoparticle surfaces are fabricated on glass slides and functionalized with target molecules. The array is then imaged in a near-field configuration and the scattered light is collected by a camera. The spatial arrangement of gold nanoparticles on the array is achieved by printing 4 nm gold seed nanoparticles from a colloidal solution using an inkjet printer into the array configuration on the surface of a glass substrate. Larger gold nanoparticles (∼100 nm) are then grown on the surface of the slide *in situ* in each of the array spots and only in the regions where the seed particles have been printed. The surface-synthesis of nanoparticles produces a final surface coverage of about 20–35% of the array spot area. A second printing step allows specific biological molecules to be delivered to each array element, addressing each spot of the array with different assays and control spots. The multi-assay array is then introduced to the array reader directly into a flow cell. The array reader monitors the scattered light intensity as target analytes flow over the entire array surface within the single flow cell. Changes in the scattered radiation intensity when compared with control spot intensity changes enable a real-time kinetic analysis of the response to be measured from which the absolute biomarker concentration can be determined.

The biophotonic surface was synthesized on the glass surface of a microscope slide using the two-step seed-mediated growth method, similar to the wet-chemical synthesis of gold rod-shaped nanoparticles (Jana et al., 2001; Murphy et al., 2005). The process involved preparation of the seed particle colloid by borohydride reduction of Au^{III} following the synthesis of Jana et al. (2001) to produce spherical seed gold nanoparticle of mean diameter 3–4 nm. In the first step these seed particles where printed onto uncoated 25 mm × 25 mm glass slides in a 12 × 8 rectangular pattern with 0.3 and 0.4 mm pitches, respectively, using a non-contact inkjet array printer (Arrayjet Aj100). The whole 96-spot array has physical dimensions of approximately 3.3 m × 2.8 mm. The array was removed from the printer and dried for approximately 20 min at 50 °C. The second step of photonic surface preparation is the particle growth procedure within each spot of the microarray. The slides are completely immersed in developing solutions containing: (i) 0.1 M CTAB, 2×10^{-4} M $HAuCl_4$, and 4×10^{-4} M ascorbic acid; or (ii) 0.1 M CTAB, 2×10^{-4} M $HAuCl_4$, 4×10^{-4} M ascorbic acid, and 2×10^{-6} M $AgNO_3$. The silver ions are added to the solution to complete the electrochemical couple between gold, silver and ascorbic acid which together with the developing time and temperature are the three important variables in the surface synthesis. These conditions affect the size and shape distribution of the particles and hence their optical properties (Noguez, 2007). The nanoparticles synthesized in each spot are covered with an extensive layer of CTAB which is removed by washing with copious amounts water and chloroform.

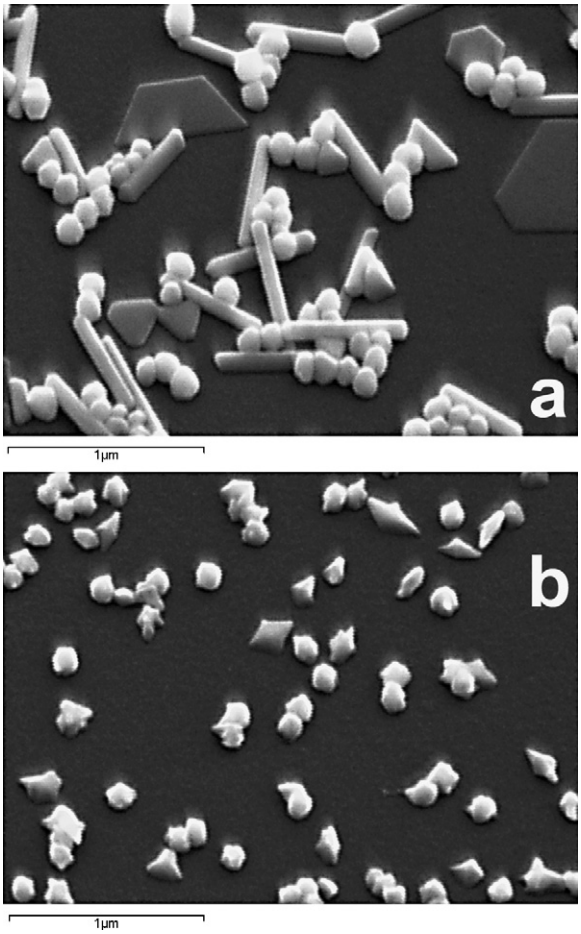

Fig. 1. SEM images of the nanoparticles developed in the growth solutions (i) and (ii), panels (a) and (b), respectively. The development in Ag^+ containing growth solution results in more uniform size and shape distribution of grown particles.

An SEM image of a typical array spot developed in growth solution (i) is shown in Fig. 1(a). A variety of nano-shapes including spherical particles, rods, and relatively flat triangular objects with different degrees of truncation are synthesized, in contrast to the preferential nanorod formation under similar conditions in the solution phase (Murphy et al., 2005). The presence of silver ions in solution during colloidal particles growth process was reported to improve yield of gold nanorods (Murphy et al., 2005), while the printed array spot development in the Ag^+-containing growth solution (ii) results in a more uniform size distribution of particles, which might be described as highly faceted gold nanocrystals, which are shown in Fig. 1(b). The array spots remain well located within the areas seeded by the array printer and do not form in the other areas of the sensor slide: nanoparticle growth is confined to the seed particles.

The biophotonic surface experiment reported here is the antibody–antigen interaction between bovine serum albumin (BSA) and anti-BSA, and human fibrinogen (HFG) and anti-HFG. In this experiment the protein is printed onto the nanofabricated gold surface and the antibody is passed over the biophotonic surface from the complete blood serum of the animal in which it was raised. The surface-synthesized particles are bio-functionalized to form a protein array in a two-step dithiobis-succinimidyl propionate (DTSP) coupling chemistry (Hermanson et al., 1992): a dithiol-link in DTSP is highly reactive towards the gold surface; and a succinimidyl ester group readily reacts with primary amino-groups of the proteins forming peptide bond, anchoring the target protein to the gold surface. The initial step may be performed in bulk solution but the slides are returned to the array printer for the target protein functionalization. A 0.5 nL sample volume of either HFG or BSA is delivered to each spot of the array. The slides are incubated in a humid atmosphere at room temperature for 40 min, and then washed to remove the excess non-bound proteins in 10 mM sodium phosphate buffer. The finished array sensor can be stored at −20 °C prior to use in the screening tests.

The multi-assay array now contains a biophotonic surface of known registration and may be used to monitor the presence of both fibrinogen and BSA from the same complex analyte solution. A simple array reader has been constructed to monitor the intensity of the scattered light from each array spot when illuminated in the near field: a schematic of the experimental arrangement is shown in Fig. 2. The array reader consists of a Dove prism with sample holder and flow cell, a digital camera (Nikon D50 with 50 mm macrolens), and a PC to process and store the data. Two continuous wave diode lasers (∼5 mW) with emission maxima at 635 and 532 nm (Scitec Instruments) are combined using a dichroic mirror and expanded through a Keplerian telescope forming ca. 4 mm diameter beam used to probe the sample. The sensor array slide is refractive index matched onto the upper surface of the Dove prism to produce the dark, near field illumination. Only the light scattered by the nanoparticles at the silica–water interface is detected by the camera, hence the nanoparticle imbued spots are observed as bright objects on a dark background.

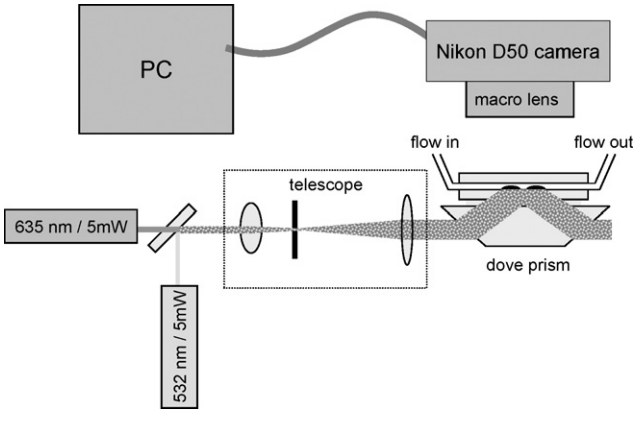

Fig. 2. Schematic diagram of the sensor array reader with two laser light sources, green (532 nm) and red (635 nm).

Images of the substrate surface are taken by the camera with 0.2 Hz acquisition rate and transferred to the computer, where the intensity of each printed array spot is followed in real-time. A typical single array spot is a ∼200 μm diameter circle which corresponds to ∼12 pixel round shape in the acquired image. The analysis software starts searching for the spots with a simple regular pattern mask, which is then refined according to the actual spot positions, and the intensities of the masked image colour channels were averaged to produce red (R) and green (G) brightness values of the array spots. Scattered radiation intensity from each of the 532 and 635 nm lasers is almost exclusively located in G and R colour channels of the image, respectively (mutual penetration <5%). The 8-bit per colour sensor of the camera is designed with non-linear response to the illumination level, and hence the useful dynamic range was limited to brightness values 0–70, roughly equivalent to ∼6-bit vertical resolution. Generally, in order to compensate for the spatial laser beam intensity distribution, the recorded transients are normalised with the initial brightness levels as recorded on the control spots of the array.

Delipidized whole antisera containing anti-HFG (developed in goat, 2.3 mg/ml antibody, 113 mg/ml other serum proteins) or anti-BSA (developed in rabbit, 3.7 mg/ml antibody, 60 mg/ml other serum proteins) were obtained from Sigma–Aldrich. During the course of bio-specific tests, the BSA and HFG antisera were diluted with 10 mM sodium phosphate buffer and normal saline buffers, respectively, to prepare two test solutions one containing ∼300 nM of anti-BSA and another containing ∼300 nM of anti-HFG. A syringe pump introduced all required solutions into the flow cell. Before the exposure of sensor arrays to each antibody containing solution they were stabilized in the corresponding buffer for the period of 10 min.

3. Results and discussion

A measure of the sensitivity of array spots may be obtained by monitoring the change in the scattered intensity recorded in each of the R or G channels when the refractive index of the bulk medium is changed in the flow cell. The smallest detectable change in the bulk refractive index (RI) is termed here the refractive index sensitivity (RIS) of the sensor and is defined as

$$\mathrm{RIS} = \sqrt{2}\sigma_I \left| \frac{\mathrm{RI}_1 - \mathrm{RI}_2}{I_1 - I_2} \right|,$$

where I is the scattered light intensity and σ_I is its standard deviation. Typically the manufactured sensor arrays demonstrated $\mathrm{RIS_G} \sim 1.5 \times 10^{-3}$ and $\mathrm{RIS_R} \sim 4 \times 10^{-3}$ per spot, when measured against the refractive index change in the solvent switch from water (RI = 1.333) to isopropyl alcohol (IPA) (RI = 1.377). There was no significant difference in RIS of surfaces produced in growth solutions (i) and (ii). For comparison the BIAcore instruments may achieve detection limit of ca. 3×10^{-7} RIU and the Texas Instrument Spreeta system reports a RIS of 10^{-6} RIU or better (Leonard et al., 2003) although the temperature compensation is important in each case because the RI of the solvent varies with the thermal coefficient of expansion and a change of 1 °C causes a baseline drift of 1×10^{-4} RIU. While such

exceptional sensitivities can be realized in instruments with a few test channels, the sensitivities of the array-based systems are a trade-of between resolution and throughput (Rich and Myszka, 2007).

The complete serum from the blood of the animal from which the antibody is raised is a complex mixture of many factors including blood globulin proteins and is an excellent benchmark mixture for pure blood. The serum containing each of the antibodies is flowed over the surface of the array in turn and the change in brightness for each spot monitored in real-time. The gold nanoparticles functionalized with selected proteins demonstrate antibody–antigen specific binding as can be seen in Fig. 3 where a key for the printing pattern for each of the proteins is also shown. The BSA and HFG are printed along each row, 1–8, of the array to improve the noise statistics and simplify the analysis. The kinetic results shown in panel (c) of Fig. 3 clearly demonstrate a significant brightness change for each of the rows functionalized with the protein congruent to their respective antibody, indicating specific antibody–antigen binding.

The intensity variation in each spot is subject to many factors, which are not associated with the specific binding events in the vicinity of biophotonic particles but still have considerable effect on the brightness of the sensor array spots: bulk solution RI and transparency, laser power fluctuations and camera collection efficiency such as shutter opening times. In addition, there is a biological noise source to the array response associated with the non-specific binding of the other components in the blood serum. Importantly, against these effects, highly specific antibody–antigen binding is observed successfully. A set of reference or control spots present in the sensor array can be used to correct the data for all the effects not associated with the target process. In the present case two sets of the sensor array spots, functionalized with BSA and HFG, are used as reciprocal references. Assuming that *non-specific* brightness variations are the same on all array spots, the difference between the observed BSA and HFG transient signals would correspond to *specific* antibody–antigen binding only. Fig. 3 presents examples of these binding transients observed upon sensor array treatment with BSA and HFG antiserum solutions.

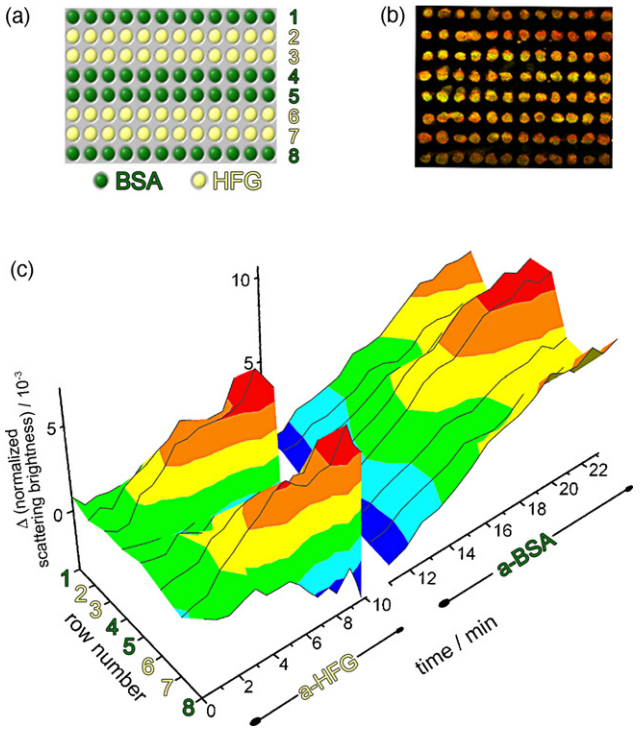

Fig. 3. Specific binding test experiment: (a) sensor array layout with the spots in rows 1, 4, 5, 8 being functionalized with BSA, and rows 2, 3, 6, 7 with HFG; (b) actual image of the sensor taken by the array reader; (c) transient scattering intensity averaged for each row of spots observed upon sequential exposure of the sensor to the anti-HFG and anti-BSA whole serum solutions; for clarity, the intensities were renormalised at $t = 11$ min to compensate for the brightness variation established in the first part of the experiment and the timescale is marked with the antisera flowed over the sensor surface at those time intervals.

Since no significant decrease in signal was observed on the timescale of the experiments when the sensor array exposed to antibody solution was treated with clean buffer, antibody–antigen dissociation was negligible and therefore the recorded transient was analysed in terms of simple adsorption kinetic model. Rate constants for the antibody–antigen binding process were derived according to the equation:

$$\frac{\mathrm{d}\vartheta}{\mathrm{d}t} = -k_\mathrm{a}[\text{antibody}]\,(\vartheta_\mathrm{m} - \vartheta)$$

where ϑ is the coverage of nanoparticles with antibodies, with ϑ_m being the maximum achievable coverage, [antibody] is the concentration of the antibody in solution, and k_a is a second-order adsorption rate constant. The observed value of k_a for BSA is $(2.5 \pm 0.6) \times 10^3\ \mathrm{M^{-1}\,s^{-1}}$, which compares favourably to reported human serum albumin antibody–protein binding rate of ca. $3 \times 10^3\ \mathrm{M^{-1}\,s^{-1}}$ measured by microbalance technique (Liu et al., 2001); the corresponding rate constant for HFG is $(6.6 \pm 0.6) \times 10^3\ \mathrm{M^{-1}\,s^{-1}}$ ($\mu \pm 2\sigma$).

4. Conclusions

The array reader has demonstrated the potential for nanoparticle light scattering to form the basis of a small-form array reader which can interrogate a biomarker array printed on an array spot forming a biophotonic surface. Critically, there is a clear specific versus non-specific binding discrimination for the antibodies contained in the whole antisera. The short-range nature of the nanoparticle plasmon field, typically penetrating one radius into the medium above the particle, is more sensitive to the near-field binding of the antibody–antigen reducing the sensitivity to non-specific binding and to variations in temperature. By contrast the continuous surface plasmon propagates several microns on the surface and penetrates typically 300 nm into the medium above the metal. The localisation of the particle plasmon appears to offer a direct advantage over the continuous surface biosensor. A nanoparticle-based biophotonic array sensor has a number of additional advantages: multiple control assays close to the target analyte assay to compensate for temperature; control spots for local laser beam intensity fluctuations; and multiple spot repetition of the same assay to improve

statistical confidence. A label-free high-throughput screening technology appears promising.

Acknowledgement

We would like to thank RCUK for a Basic Technology Grant "2D Attogram Surface Plasmon Imaging", grant number: EP/C52389X/1.

References

Haes, A.J., Duyne, R.P.V., 2004. Anal. Bioanal. Chem. 379 (7-8), 920–930.
Haes, A.J., Stuart, D.A., Nie, S., Duyne, R.P.V., 2004. J. Fluores. 14 (4), 355–367.
Heaton, R.J., Peterson, A.W., Georgiadis, R.M., 2001. Proc. Natl. Acad. Sci. U.S.A. 98 (7), 3701–3704.
Hermanson, G.T., Mallia, A.K., Smith, P.K., 1992. Immobilized Affinity Ligand Techniques. Academic Press.
Jana, N.R., Gearheart, L., Murphy, C.J., 2001. J. Phys. Chem. B 105, 4065–4067.
Lee, H.J., Nedelkov, D., Corn, R.M., 2006. Anal. Chem. 78, 6504–6510.
Leonard, P., Hearty, S., Brennan, J., Dunne, L., Quinn, J., Chakraborty, T., O'Kennedy, R., 2003. Enzyme Microb. Technol. 32, 3–13.
Liu, Y.-C., Wang, C.-M., Hsiung, K.-P., 2001. Anal. Biochem. 299, 130–135.
McFarland, A.D., Duyne, R.P.V., 2003. Nano Lett. 3 (8), 1057–1062.
Murphy, C.J., Sau, T.K., Gole, A.M., Orendorff, C.J., Gao, J., Gou, L., Hunyadi, S.E., Li, T., 2005. J. Phys. Chem. B 109, 13857–13870.
Noguez, C., 2007. J. Phys. Chem. C 111 (10), 3806–3819.
Phillips, K.S., Wilkop, T., Wu, J.-J., Al-Kaysi, R.O., Cheng, Q., 2006. J. Am. Chem. Soc. 128, 9590–9591.
Rich, R.L., Myszka, D.G., 2007. Anal. Biochem. 361, 1–6.
Stuart, D.A., Haes, A., McFarland, A.D., Nie, S., Duyne, R.P.V., 2004. Proc. SPIE 5327, 60–73.